ENERGY DISSIPATION IN SUBSTORMS

L. A. Weiss, [1] P. H. Reiff, [1] J. J. Moses, [1] R. A. Heelis[2] and B. D. Moore[1]

[1]Department of Space Physics and Astronomy, Rice University, Houston, Texas
[2]University of Texas, Dallas, Texas

ABSTRACT

The energy dissipated by substorms is manifested in several ways: the Joule dissipation in the ionosphere; the energization of the ring current by the injection of plasma sheet particles; auroral election and ion acceleration; plasmoid ejection; and plasma sheet ion heating during the recovery phase. Each of these energy dissipation mechanisms is discussed, a 'rule of thumb' formula is given, and a typical dissipation rate and total energy expenditure is estimated. We find that the total energy dissipated as Joule heat ($\sim 2 \times 10^{15}$ W) is about twice the ring current injection term, and may be even larger if small-scale effects are included. The energy expended in auroral electron precipitation, on the other hand, is smaller than the Joule heating by a factor of five. We estimate that the energy expended in refilling and heating the plasma sheet is $\sim 5 \times 10^{14}$ J, while the energy lost due to plasmoid ejection is between $\sim 10^{13}$ - 10^{14} J.

Keywords: substorms, energy dissipation, Joule heating

1. INTRODUCTION

During a substorm, energy previously transmitted from the solar wind and stored in the magnetosphere is dissipated in the inner magnetosphere and auroral ionosphere, in the form of ring current energization, Joule heating, and particle precipitation, and in the magnetotail, in the form of plasma sheet ion heating and plasmoid ejection. In general, energy dissipation in the inner magnetosphere and auroral ionosphere is more easily monitored and estimated than energy dissipation in the magnetotail. The global energetics of the magnetosphere have been reviewed by *Akasofu* [Ref. 1] and *Stern* [Ref. 2], and a number of studies have compared the magnetospheric energy input and dissipation rates due to Joule heating, particle precipitation, and ring current energization [Ref. 1, 3.- 7]. *Baker et al.* [Ref. 8] have performed an especially detailed study of the storage of solar wind energy in the magnetotail and the pre- and post-expansion onset dissipation of the stored energy. Our purpose in this paper is to briefly review magnetospheric energy input and substorm energy dissipation mechanisms, provide a 'rule of thumb' method for estimating the power and/or total energy expended by each mechanism, and to summarize estimates of these quantities for both typical and large substorm events.

2. SOLAR WIND ENERGY INPUT

The electromagnetic energy available to the magnetosphere, and hence available for dissipation, is supplied by the solar wind. Numerous studies have shown that the total rate of energy transfer from the solar wind to the magnetosphere is largely controlled by the southward component of the IMF [e.g., Ref. 9]. The potential drop associated with viscous processes is typically small (10 kV or less) [Ref. 10, 11, 12], with the largest (~20 kV) viscous potentials occurring during cases of large northward IMF [Ref. 13]. With a number of simplifying assumptions, the energy transfer rate at the magnetopause can be approximated by [Ref. 2]

$$U_{sw} = I_{ct}\ \Phi_{pc} \qquad (1)$$

where I_{ct} is the cross-tail current and the cross-polar cap potential drop, Φ_{pc}, can be estimated by [Ref. 12]

$$\Phi_{pc} = f\, v\, B \sin^2\left(\frac{\theta}{2}\right) 2\, R_{CF} \qquad (2)$$

Here v and B are the solar-wind velocity and magnetic field strength (with a saturation value of B = 10.8 nT), R_{CF} is the pressure-dependent standoff distance, θ is $\cos^{-1}(Bz/|B|)$, and f is an empirical coefficient of value 0.31, as shown in Fig.1. A dayside cross-section of the magnetosphere ~3 R_{CF} implies a global merging efficiency of about 0.20. For a cross-tail current of $\sim 1 \times 10^7$ A and a maximum polar cap potential drop of 200 kV (pathological cases have been observed as high as 250 kV), the rate of energy input from the solar wind

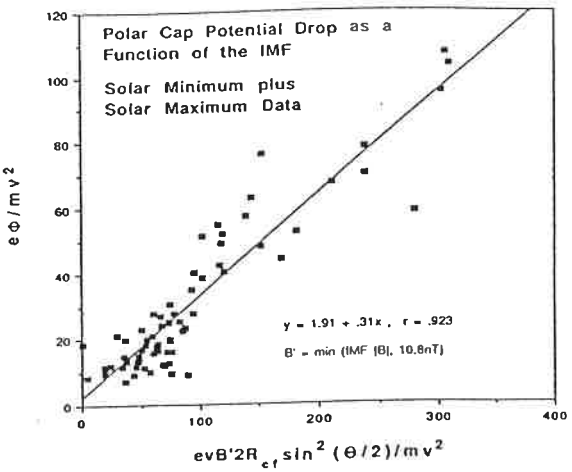

Fig. 1: Correlation of the normalized cross-polar cap potential drop $e\Phi / mv^2$ with equation (2) [Ref. 12].

is $U_{SW} \sim 2 \times 10^{12}$ W. More typically, $U_{sw} \sim 5 \times 10^{11}$W. This rate of energy transfer represents about 5% of the total solar wind power incident on the magnetosphere, given by

$$U_{sw(total)} = \frac{1}{2} \rho \, v^3 \, L^2_{CF} \qquad (3)$$

where ρ and v are the solar wind mass density and velocity, and L_{CF} is the Chapman-Ferraro scale length (~30 R_E). For average solar wind conditions, $\rho \approx 8.4 \times 10^{-21}$ kg/m^3, $v \approx 4 \times 10^5$ m/s, and thus the total solar wind energy rate available is $U_{sw(total)} \sim 10^{13}$ W, increasing by over an order of magnitude in high speed streams.

Perreault and Akasofu [Ref. 14] and *Akasofu* [Ref. 1, 15] have shown that the energy transfer rate between the solar wind and the magnetosphere is also well approximated by the empirical function ε, in units of ergs/s, given by

$$\varepsilon(t) = v B^2 \sin^4\left(\frac{\theta}{2}\right) l_0^2 \qquad (4)$$

where l_0 is a constant ≈ 7 R_E, θ is the angle between the GSM z-direction and the projection of the IMF in the y-z plane, and all quantities are in cgs units [Ref. 2]. It should be noted however, that this formula does not include energy transfer across the LLBL, or energy transfer by particles. Typically, $\varepsilon \sim 0\text{-}5 \times 10^{11}$ W. In the large CDAW 6 substorm on March 22, 1979, *Baker et al.* [Ref. 8] calculated an average value of ε of $\sim 4 \times 10^{12}$ W. Several studies showing clear correlations between ε and Akasofu's estimate of the total output rate, U_T (a combination of energy dissipation due to Joule heating, ring current dissipation, and particle precipitation) have emphasized the directly-driven aspect of magnetospheric substorms by showing the similarity between their temporal profiles [Ref. 1, 15]. (See, however, Ref. 23). Other authors have emphasized that both directly-driven and unloading aspects are necessary components of substorm energy dissipation [Ref. 16, 8]. Most recently, the successful prediction of the AE index from solar wind parameters by *Goertz et al.* [Ref. 17] has provided a powerful case for the directly-driven aspect of substorms, and includes the effects of wave travel times, tail energy storage and conductivity feedback.

3. ENERGY STORAGE IN THE MAGNETOTAIL

During periods of southward IMF, electromagnetic energy is extracted from the solar wind kinetic energy and stored as enhanced magnetic-field energy density in the tail lobes. As shown by the superposed epoch averages of *Caan et al.* [Ref. 18] in Fig. 2, the tail magnetic field energy increases prior to the onset of a substorm (growth phase) and decreases rapidly during the expansion phase. The rate of change of magnetic flux in the lobe could in principle be estimated from the dayside merging rate ,R, and the tail reconnection rate ,*R*, since

$$\frac{d\Phi_{tail}}{dt} = R_{day} - R_{tail} \qquad (5)$$

where Φ_{tail} is the tail lobe magnetic flux, but in practice the tail reconnection rate is not easy to determine. The change in tail flux can also be estimated by measuring the tail lobe field strength as a function of time, and estimating the cross-sectional area of the magnetotail Using this method, *Baker et al.* [Ref. 8, 19] estimated the total energy gain for the March 31 CDAW 6 event to be ~4.6×10^{15} J. Although an independent method of monitoring the radius of the tail does not presently exist, it can be estimated from the component of the solar wind pressure normal to the tail boundary [Ref. 20] including the effect of the magnetotail flaring [Ref. 21]. Another way to quantify the amount of magnetic energy stored

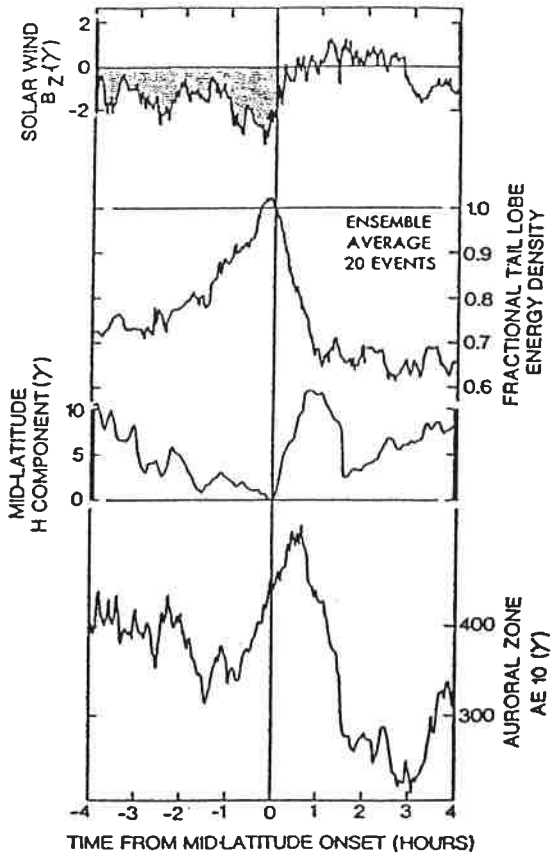

Fig. 2: Superposed analysis of the IMF Bz, tail lobe energy density, mid-latitude ground magnetic perturbations, and the AE index [Ref. 23].

in the tail is from the total magnetic flux contained within the polar cap identified in satellite images (assuming that the boundary of the luminosity corresponds to the boundary of open field lines) [Ref. 22]; [*Lockwood*, personal communication, 1991]. *Frank and Craven* [Ref. 22] determined the rate of increase of magnetic energy in the magnetotail during the growth phase of a substorm to be ~2×10^{12} W using this method, with a similar amount released in the expansion phase. In the canonical (i.e., superposed epoch) substorm of Ref. 18, the total energy stored in the magnetotail during the growth phase is shown to be ~10^{15} J, with tail energy density rising about 30% in the growth phase and falling the about same amount in the expansion phase.

4. ENERGY DISSIPATION MECHANISMS

4.1. *Ring Current Injection*

Energy stored in the magnetotail is partially converted into particle energy in the ring current after the onset of a substorm. Plasma is injected into the ring current during the dipolarization phase, resulting in strongly negative (up to ~-100 nT) values of Dst. The energy contained in the ring current particles was first estimated as a function of Dst (ΔB) by *Dessler and Parker* [Ref. 24] as

$$\frac{E_{rc}}{E_m} = -\frac{3}{2}\frac{\Delta B}{B_0} \qquad (6)$$

where E_m is the total dipolar geomagnetic field energy, E_{rc} is the total particle energy parallel to the magnetic field, and B_0 is the surface equatorial field intensity. With $B_0 = 3 \times 10^4$ nT, $E_m = 8 \times 10^{17}$ J and $\Delta B = 100$ nT, the total energy in the ring current is given by $E_{rc} \sim 4 \times 10^{15}$ J. This value is only an estimate, however, since the field can be substantially distorted during a magnetic storm; more accurate

calculations using open, distended magnetic fields are in progress [*Maltsev*, personal communication, 1992]. In the recovery phase of a magnetic storm, the particle energy stored in the ring current is dissipated as heat and light by precipitation of the ring-current particles into the atmosphere and by charge exchange between ring-current particles and neutral atoms. In general, the decay of the ring current is rapid in the early recovery phase and more gradual in the later stages of the storm recovery, indicating a non-uniform ring current particle lifetime that may be dependent on the input energy rate [Ref. 1] or on the composition of the ring current if the main process removing its particles is charge exchange [Ref. 25]. The ring current injection rate is approximately

$$U_{rc} = -4 \times 10^{13} \left[\frac{\partial Dst}{\partial t} + \frac{Dst}{\tau_r} \right] \qquad (7)$$

[Ref. 1] where τ_r is the ring current particle lifetime and Dst (in nT) has been suitably corrected for effects due to pressure variations in the solar wind [Ref. 26, 27]. Measurements of ΔB should also be corrected for the effects of currents induced in the solid Earth [Ref. 28], as discussed in Ref. 2.

The development of the substorm ring current and energy injection rate was modeled by *Harel et al.* [Ref. 4] using the Rice Convection Model [Ref. 29]. The results of their modeling, shown in Fig. 3, indicate an energy input rate of $U_{rc} \sim 1 \times 10^{11}$ W and a total change in ring current energy during the substorm of $\sim 1.4 \times 10^{15}$ J for a polar cap potential drop of 80 kV. The largest Dst excursion in recent times was during the storm of March 14, 1989, where the minimum Dst reached -600 nT, after the polar cap potential averaged nearly 200 kV for over 12 hours [*R. A. Wolf*, personal communication, 1992]. Even in that event, the fastest rate of Dst decrease was about 350 nT over 7 hours, or an energy injection rate of about 6×10^{11} W.

4.2. *Auroral Electron Precipitation and Upflowing Ions*

A relatively small, but well estimated, percentage of the global

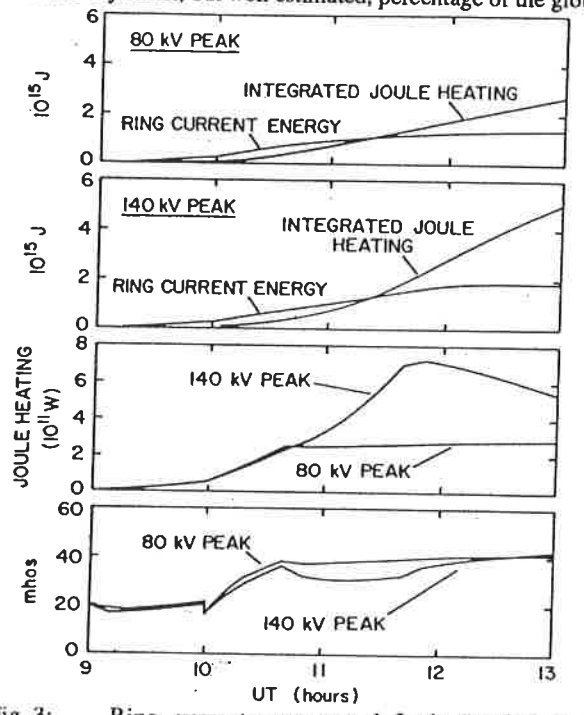

Fig. 3: Ring current energy and Joule heating as a function of UT. Results are shown for model calculations using 80 kV and 140 kV peak cross-polar cap potential drops. The bottom panel shows the ratio of the Joule heating to the square of the polar cap potential drop [Ref. 4].

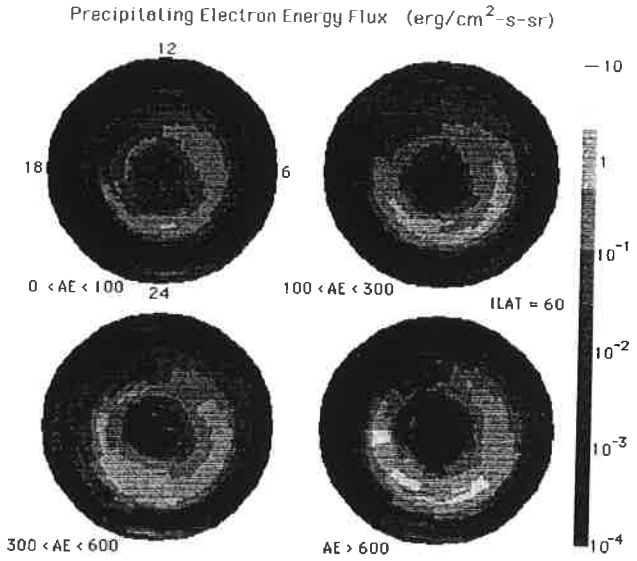

Fig. 4: Contour plots of precipitating electron energy flux sorted according to the AE index. [data from Ref. 31]

energy budget is deposited in the atmosphere by precipitating auroral electrons. *Spiro et al.* [Ref. 30] correlated the average global distributions of precipitating electron energy flux and average energy (using AE-C and -D satellite data) with the AE index, and showed that the power from precipitated auroral electrons could be approximated by

$$U_a = [1.75 \left(\frac{AE}{100\ nT} \right) + 1.6] \times 10^{10}\ W \qquad (8)$$

For our canonical substorm with AE of ~500 nT [Ref. 18] (Fig. 2), the typical energy deposition rate due to particle precipitation is $U_a \sim 1 \times 10^{11}$ W with a total deposition over 1 hr of 3×10^{14} J. In a larger substorm such as the March 22, event [Ref. 31] these values may approach 5×10^{11} W and 2×10^{15} J, respectively. The electron energy flux as a function of invariant latitude and local time for four different AE bins is replotted from [Ref. 30] in Figure 4 (see also Ref. 32, 33). We stress that AE does a better job of ordering the electron precipitation than Kp [Ref. 30], and thus we do not recommend using a Kp-indexed estimate of the particle precipitation; frankly, the use of a 3-hour index to order *any* substorm-related parameter is unlikely to be accurate. *Hardy et al.* [Ref. 34] showed that the average precipitating ion energy flux is only ~11-17% of the electron energy flux.

The power expended in accelerating ions out of the ionosphere during auroral substorms is much smaller than that spent on precipitating electrons since ions have small mobilities and relatively low fluxes. *Yau et al.* [Ref. 35] used EICS data to determine the distribution and variability of upflowing ionospheric ions over the auroral zone and polar cap. They estimated the total ion outflow (H^+ and O^+) was 1.5×10^{26} ions/s at active times ($3 \le Kp \le 5$) and 5×10^{25} ions/s at quiet times ($Kp \le 2$) for solar maximum conditions. Using an average ion outflow of 1×10^{26} ions/s and an typical energy of 500 eV, power dissipated by upward ion flow in the auroral zone is $U_i \sim 1 \times 10^{10}$ W. The net flux associated with near-thermal ion outflows [Ref. 36] is over an order of magnitude larger; however, the considerably lower mean energy implies that the energy flux associated with thermal ions is quite small. Terrestrial ions are important in determining the total magnetospheric plasma content and the subsequent acceleration of these ions back toward the earth (forming part of the ring current) may also result in substantial energy redistribution [Ref. 37].

4.3. *Joule Heating*

One of the most important modes of energy transfer from the magnetosphere to the ionosphere during substorms is Joule heating. The global Joule heating rate due to an ionospheric current density **J** is given by

$$U_{Jh} = \int \mathbf{E}' \cdot \mathbf{J}\, dV = \int \Sigma_P\, E'^2 dx\, dy \qquad (9)$$

where the effective electric field is given by $\mathbf{E}' = \mathbf{E} + \mathbf{u} \times \mathbf{B}$ (with **u** the neutral wind, typically ignored in calculations), Σ_p is the height-integrated Pedersen conductivity, and the integration covers latitudes >50° IL. Statistical studies of hemispheric Joule heating rates have been conducted by a number of authors [e.g., Ref. 6, 38, 39, 40, 41] using average measurements of ionospheric electric fields and models or calculations of global Pedersen conductances; as an example, the distribution of Joule heating in the northern hemisphere calculated by *Heelis* [Ref. 40] is shown in Fig. 5. Difficulties

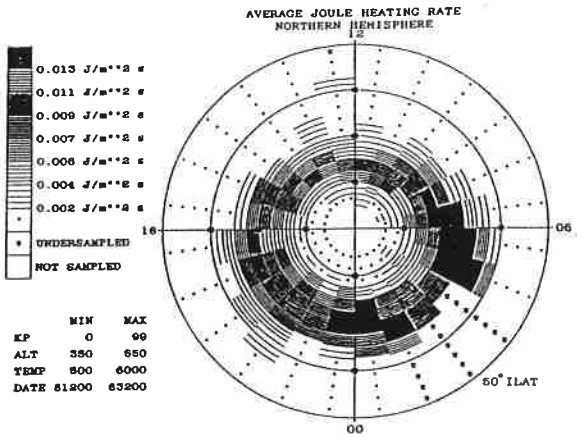

Fig. 5: The height-integrated northern-hemisphere Joule heating rate computed from the Pedersen conductance and the square of the perpendicular electric field (determined from DE-2 satellite measurements) [Ref. 40].

in accurately estimating Joule heating rates arise because the electric field and conductivity are rarely known simultaneously and the average value of E^2 is typically larger than the square of the average value of E [Ref. 39, 40]. Figure 6, from *Foster* [Ref. 39], shows the energy dissipation by Joule heating as a function of Kp for different seasons as well as the energy dissipation due to particle precipitation estimated by *Spiro et al.* [Ref. 30]. *Ahn et al.* [Ref. 42] showed that the typical Joule heating rate is nearly linear with AE or AL ($U_{Jh} \sim 2.3 \times 10^8$ AE). Individual event studies [e.g., Ref. 4, 8, 43] have resulted in estimates of the total Joule heating rate between $\sim 8 \times 10^{10}$ and 1.8×10^{12} W. *Harel et al* [Ref. 4] showed analytically that the Joule heating rate is about twice the energy dissipated in the ring current, and can be approximated by

$$U_{Jh} = \Sigma'_P \Phi_{pc}^2 \qquad (10)$$

where Σ'_P is an effective global ionospheric Pedersen conductance of ~30 mho [see bottom panel of Figure 3].

As an example of the effect of small-scale structure on Joule dissipation in substorms, we have fit an expanding-contracting polar cap (ECPC) model to a DE-2 satellite pass during a small (AE = 500 nT) substorm on October 6, 1981, when tail econnection was occurring. Ion flow measurements for this pass are shown in Fig. 8(a). The region of eastward flow at ~2230 MLT and 68° IL, which occurs at substorm expansion, is on closed field lines within the discrete auroral region

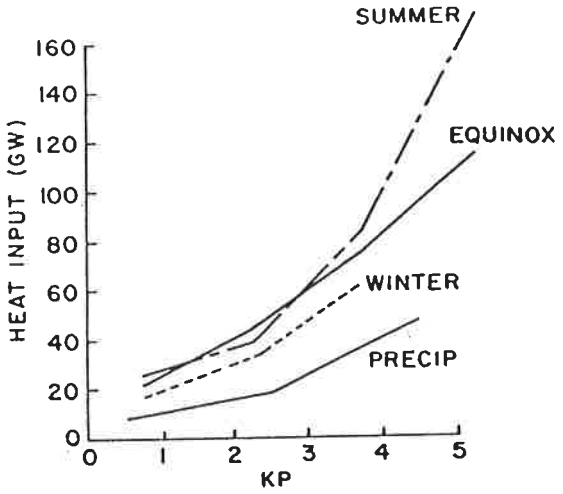

Fig. 6: Single hemisphere energy input due to Joule heating as a function of Kp. For comparison, the energy input due to electron precipitation estimated by [Ref. 30] is also shown [Ref. 39].

and thus may be indicative of outflow equatorward of the footprint of the tail reconnection line. When the flow measurements are fit to the ECPC model [Ref. 44, 45] the convection pattern shown in Fig. 8(b) results. The best fit to the flow velocities is given by a dayside merging gap potential of 50 kV and a nightside gap potential of 10 kV (indicative of the tail reconnection rate). Using statistical models of the conductivity from the data of *Spiro et al* [Ref. 30],we obtain a Joule heating rate in the vicinity of the nightside gap of $U_{Jh} = 2.8 \times 10^9$ W, which accounts for essentially all of the northern hemisphere nightside Joule heating.

We also calculate the Joule heating along the spacecraft track by combining 0.5 sec resolution measurements of the ion flow velocity and 1 sec resolution values of the conductivity calculated from the precipitating electron fluxes [Ref. 9] The Joule heating rate integrated along the spacecraft track within the nightside gap is U_{Jh} ~25 kW/m. If the flow channel extends 1000 km, the total Joule dissipation rate is 2.5×10^{10} W, or about a factor of 10 larger than the low-resolution calculation suggests (Fig. 7). These results indicate that local Joule heating within narrow auroral features can be very significant to the total energy dissipation in substorms.

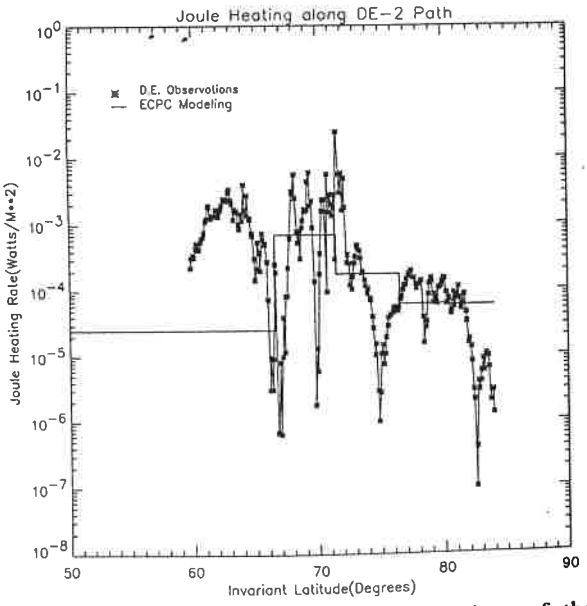

Fig. 7: Low- and high-resolution calculations of the integrated Joule heating rate along the DE-2 path.

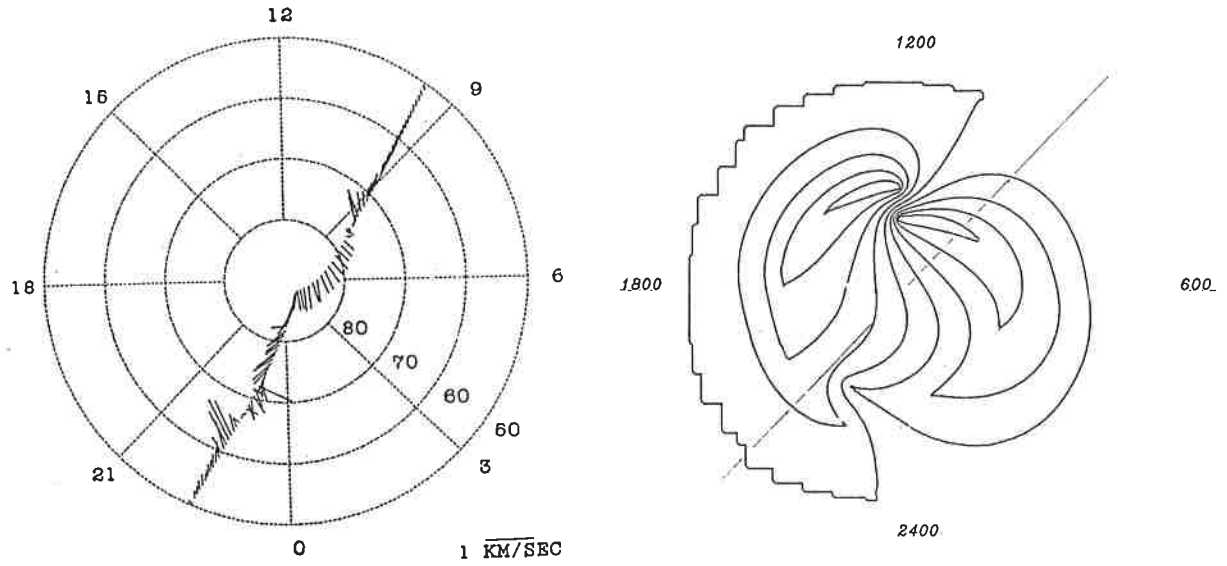

Fig.8 (a) Ion velocity measurements from a DE-2 satellite pass on October 6, 1981 (Orbit 948). (b) ECPC model convection pattern corresponding to (a).

4.4. *Plasmoid Ejection*

In the most frequently adopted substorm model, a near-Earth neutral line is formed between -10 to -20 R_E at substorm onset causing ring current injection, particle energization, and the severance of the plasma sheet to form a plasmoid [Ref. 46, 47]. Rapid plasma flow away from the Earth and southward magnetic fields in the distant tail (observed by ISEE 3) and in the mid-tail (observed by IMP 8) have been interpreted as evidence of plasmoid formation, [e.g., Ref. 48,-52]. The rate of energy loss due to plasmoid ejection can be estimated from

$$U_{plasmoid} = \frac{1}{2}\rho\, v^3 A \qquad (11)$$

where ρ is the average mass density of the plasmoid, v is its velocity downtail, and A is its cross-sectional area. For an average downtail velocity of 400 km/s, ρ =0.5 cm^{-3}, and a plasmoid cross-section of $2 \times 30\ R_E$ [Ref. 20, 47, 50], the energy loss rate is ~5×10^{10} W. Assuming a duration of 6 minutes, the total energy in a single plasmoid is ~2×10^{13} J. For a large event, the velocity can increase to 1200 km/s [Ref. 20], yielding rates of ~1×10^{12} W and ~4×10^{14} J, respectively. *Slavin et al.* [Ref. 49] also estimated the energy loss rate due to plasma flow away from Earth in the distant plasma sheet as a function of AE, obtaining 6 - 12×10^{10} W.

4.5. *Plasma Sheet Heating*

On the earthward side of a near-Earth neutral line, the reconnection model predicts the earthward movement of energetic plasma and the dipolarization of the field in the inner magnetotail during the recovery phase. It is well known that the plasma sheet thins during the growth phase and expands in the recovery phase, with the post-recovery plasma sheet considerably hotter than in quiet times. *Hardy et al.* [Ref. 53] showed an increase by nearly a factor of 10 of electron and ion temperatures in the plasma sheet during recovery phase at lunar distance. Nearer the earth, *Christon et al.* [Ref. 54] showed that plasma sheet temperature increases (decreases) correspond to times of increasing (decreasing) AE. *Baumjohann et al.* [Ref. 55, 56] show that temperatures in both the plasma sheet and the plasma sheet boundary layer (PSBL) are a strong function of AE. For a given AE, they showed higher PSBL temperatures (by a factor of 2) associated with transitions in which the PSBL overtook the spacecraft, presumably plasma sheet expansions, compared to transitions where the spacecraft went from the plasma sheet to lobe. If we approximate the plasma sheet by a wedge with a triangular cross-section in the noon-midnight plane with inner edge at 8 R_E, a vertical extent there of 8 R_E decreasing to zero thickness at 20 R_E, covering a width of 30 R_E in the y-direction, a density of 0.4 cm^{-3} and temperature 2.5 keV [Ref. 56] we get a total energy content ~6×10^{13} J. If during substorm expansions the plasma sheet expands in volume by a factor of 5 (mostly in length) and in average temperature by a factor of 2, this corresponds to an energy budget ~5×10^{14} J in the course of a substorm. If this occurs in 20 minutes, the average energization is about 3×10^{11} W.

5. SUMMARY

Knowledge of the magnetospheric energy budget, namely the various modes of energy input and dissipation, is essential to the study of magnetospheric substorms. Table 1 summarizes the energy sources and sinks reviewed in this paper, lists 'rule of thumb' formulas for each mechanism, and shows the power and total energy expenditure for both typical and large events. Assimilating the material presented in this review provides some interesting perspectives on the partitioning and redistribution of energy during a substorm. The energy derived from the solar wind is not, of course, distributed in series through different elements of the magnetosphere - ionosphere system, but it is useful to summarize the self-consistent nature of the energy available and redistributed in each element. We would like to point out, however, that the estimates in the table have been compiled from many sources and thus may not be mutually consistent.

If we assume that the solar wind energy input rate prior to a typical (large) substorm is ~5×10^{11} W (4×10^{12} W) over a period of 1 hour (2 hours), then the total energy transferred to the magnetosphere is ~2×10^{15} J (3×10^{16} J), a substantial fraction of which is stored as magnetic energy density in the tail lobes. During the growth phase, the electric field in the system increases, as well as the ionospheric conductivity, leading to enhanced Joule dissipation in the ionosphere [Ref. 57]. During the expansion phase the tail energy is redistributed in the system by particle heating and plasma injection to the ring current, and by tailward ejection of a plasmoid. Statistical and case studies indicate that the predominant energy dissipation mechanism is Joule heating, which accounts for nearly 2×10^{15} J (8×10^{15} J). We note that the inclusion of local Joule dissipation within small but intense auroral features may increase the total Joule heating rate by a factor of 10. Energization of the ring current requires 10^{15} J

TABLE 1.

Energy Source or Sink	Rule of Thumb Formula	Power (W)		Total Energy (J)	
		Typical	Large	Typical	Large
Solar Wind Input	$\varepsilon(\text{ergs/s}) = v B^2 \sin^4\left(\frac{\theta}{2}\right) l_0^2$	5×10^{11}	4×10^{12}	$1.8 \cdot 10^{15}$ 2×10^{15}	3×10^{16}
Tail Storage	$\frac{d\Phi_{pc}}{dt} = R_{day} - R_{tail}$ $B_{pc}A_{pc} = B_{lobe}A_{lobe}$	5×10^{11}	2×10^{12}	1×10^{15}	1×10^{16}
Ring Current	$E_{rc} = -1.5\,(\Delta B / B_0)\,E_m$ $U_{rc} = 4 \times 10^{13}\left[\frac{\partial Dst}{\partial t} + \frac{Dst}{\tau_r}\right]$	4×10^{11}	1×10^{12}	0.1×10^{15} 1×10^{15}	4×10^{15}
Electron Precipitation	$U_a = [\,1.75\,(AE / 100\,nT) + 1.6] \times 10^{10}$ W	1×10^{11}	5×10^{11}	$0.3 \cdot 10^{15}$ 4×10^{14}	2×10^{15}
Upflowing Ions		1×10^{10}	2×10^{10}	3×10^{13}	6×10^{13}
Joule Heating	$U_{Jh} = 2.3 \times 10^8$ AE $U_{Jh} \approx 30\,\Phi_{pc}^2$	$7.3 \cdot 10^{10}$ 8×10^{10}	2×10^{12}	$1 \cdot 10^{15}$ 2×10^{15}	8×10^{15}
Plasmoid Ejection	$U_{plasmoid} = \frac{1}{2}\rho\, v^3 A$	5×10^{10}	1×10^{12}	2×10^{13} ?	4×10^{14}
Plasma Sheet Heating		1×10^{11}	6×10^{11}	2×10^{14} ?	1×10^{15}

(4×10^{15} J), a factor of 2 (4) greater than that involved in heating the plasma sheet and nearly 50 (10) times more than that released in plasmoid ejection. The energy in Joule heating is roughly 2-5 times that expended in auroral electron precipitation. Finally, the energy of the ring current is dissipated as energetic neutrals and as heat in the ionophere by particle precipitation.

ACKNOWLEDGMENTS

This work was supported by the National Science Foundation under grant ATM90-22662, and by NASA under grants NAGW-1655 and NAG5-775 and at the University of Texas at Dallas under grant NAG5-305. The authors would like to thank David Stern, Dick Wolf, and Cheryl Huang for their valuable comments.

REFERENCES

1. Akasofu, S-I 1981, Energy coupling between the solar wind and the magnetosphere, *Space Sci. Rev.*, **28,** 121-190.

2. Stern, D P 1984, Energetics of the magnetosphere, *Space Sci. Rev.*, **39,** 193-213.

3. Akasofu, S I 1983, Solar-wind disturbances and the solar wind-magnetosphere energy coupling function, *Spac. Sci. R*,ev., **34,** 185.

4. Harel, M, *& al.* 1981, Quantitative simulation of a magnetospheric substorm 2, comparison with observations, *J. Geophys. Res.*, **86,** 2242-2260.

5. Baker, D N, *& al.* 1983, An ISEE-3 high time resolution study of interplanetary parameter correlations with magnetospheric activity, *J. Geophys. Res.*, **88,** 6230.

6. Baumjohann, W & Kamide, Y 1984, Hemispherical Joule heating and the AE indices, *J. Geophys. Res.*, **89,** 383.

7. Tsurutani, B T, *& al.* 1985, Coupling between the solar wind and the magnetosphere: CDAW-6, *J. Geophys. Res.*, **90,** 1191-1199.

8. Baker, D N, *& al.* 1985, Magnetotail energy storage and release during the CDAW 6 substorm analysis interval, *J. Geophys. Res.*, **90,** 1205-1216.

9. Reiff, P H 1984, Evidence of magnetic merging from low-latitude spacecraft and ground-based observations, *Magnetic Reconnection in Space and Laboratory Plasmas*, , 104-113.

10. Hill, T W 1979, Rates of mass, momentum, and energy transfer at the magnetopause, in *Proceedings of Magnetospheric Boundary Layers Conference*, Alpbach, Austria: ESA SP-148.

11. Reiff, P H & Luhmann, J G 1986, Solar wind control of the polar cap voltage, in *Solar Wind-Magnetosphere Coupling*, Y.K.a.J.A. Slavin, Editor, Astrophysics and Space Science Library, Terra Sci. Publ. Co., Tokyo, 453-476.

12. Moses, J J & Reiff, P H 1991, Polar cap convection: Steady state and dynamic effects, in *Magnetospheric Substorms*, Y. Kamide, Editor, Geophy. Monogr., **64,** AGU Press, Washington,

13. Heelis, R A, *& al.* 1986, Ionospheric convection signatures observed by DE 2 during northward interplanetary magnetic field, *J. Geophys. Res.* , **91,** 5817-5830.

14. Perreault, P & Akasofu, S-I 1978, A study of geomagnetic storms, *Geophys. J. Roy. Astron. Soc.*, **54,** 547.

15. Akasofu, S-I 1979, Interplanetary energy flux associated with magnetospheric substorms, *Planet. Space Sci.*, **27,** 4, 425-471.

16. Zwickl, R D, *& al.* 1987, An evaluation of the total magnetospheric energy output parameter, U_T, in *Magnetotail*

Physics, A.T.Y. Lui, Editor, The Johns Hopkins University Press, Baltimore, 155-159.

17. Goertz, C K, *& al.* 1992, Prediction of geomagnetic activity, *J. Geophys. Res.*, **87,** in press.

18. Caan, M N, *& al.* 1975, Substorm and interplanetary magnetic field effects on the geomagnetic tail lobes, *J. Geophys. Res.* , **80,** 191.

19. Baker, D N, *& al.* 1981, Global properties of the magnetosphere during a substorm growth phase: a case study, *J. Geophys. Res.*, **86,** 8941.

20. Fairfield, D H, *& al.* 1989, Substorms, plasmoids, flux ropes, and magnetotail flux loss on March 25, 1983: CDAW 8, *J. Geophys. Res.*, **94,** 15135-15152.

21. Coroniti, F V & Kennel, C F 1972, Changes in magnetospheric configuration during the substorm growth phase, *J. Geophys. Res.*, **77,** 3361-3370.

22. Frank, L A & Craven, J D 1988, Imaging results from Dynamic Explorer 1, *Rev. Geophys.*, **26,** 2, 249-283.

23. Lui, A T Y 1992, What determines the intensity of magnetospheric substorms?, *J. Atm. Terr. Phys.*, submitted.

24. Dessler, A J & Parker, E N 1959, Hydromagnetic theory of geomagnetic storms, *J. Geophys. Res.*, **64,** 2239-2252.

25. Tinsley, B A 1976, Evidence that the recovery phase ring current consists of helium ions, *J. Geophys. Res.*, **81,** 6193-6196.

26. Siscoe, G L, *& al.* 1968, Relation between geomagnetic sudden impulses and solar wind pressure changes -- an experimental investigation, *J. Geophys. Res.*, **73,** 4869.

27. Carovillano, R L & Siscoe, G L 1973, Energy and momentum theorems in magnetospheric processes, *Rev. Geophys. Space Phys.*, **11,** 289-353.

28. Langel, R A & Estes, R H 1983, *Large-Scale, near-Earth magnetic fields from external sources and the corresponding induced internal sources,* , NASA Technical memorandum, **TM-85012,** NASA, Washington,

29. Wolf, R A 1974, Calculations of magnetospheric electric fields, in *Magnetospheric Physics,* B.M. McCormac, Editor, D. Reidel, Dordrecht, Netherlands, 167-177.

30. Spiro, R W, *& al.* 1982, Precipitating electron energy flux and auroral zone conductances -- an empirical model, *J. Geophys. Res.*, **87,** 8215.

31. McPherron, R L & Manka, R H 1985, Dynamics of the 1054 UT March 22, 1979 substorm event: CDAW-6, *J. Geophys. Res.*, **90,** 1175-1190.

32. Fuller-Rowell, T J & Evans, D S 1987, Height-integrated Pedersen and Hall conductivity patterns inferred from the TIROS-NOAA satellite data, *J. Geophys. Res.*, **92,** 7606-7618.

33. Hardy, D A, *& al.* 1987, Statistical and functional representations of the pattern of auroral energy flux, number flux, and conductivity, *J. Geophys. Res.*, **92,** 12275-12294.

34. Hardy, D A, *& al.* 1989, A statistical model of auroral ion precipitation, *J. Geophys. Res.*, **94,** 370-392.

35. Yau, A W, *& al.* 1985, Energetic auroral and polar ion outflow at DE 1 altitudes: magnitude, composition, magnetic activity dependence, and long-term variations, *J. Geophys. Res.* , **90,** 8417-8432.

36. Chappell, C R 1988, The terrestrial plasma source: A new perspective in solar-terrestrial processes from Dynamics Explorer, *Rev. Geophys.*, **26,** 229-248.

37. Young, D T, *& al.* 1982, Correlations of magnetospheric ion composition with geomagnetic and solar activity, *J. Geophys. Res.*, **87,** 9077.

38. Banks, P M, *& al.* 1981, Chatanika radar observations relating to the latitudinal and local time variations of Joule heating, *J. Geophys. Res.*, **86,** 6869.

39. Foster, J C, *& al.* 1983, Joule heating at high latitudes, *J. Geophys. Res.*, **88,** 4885.

40. Heelis, R A & Coley, W R 1988, Global and local Joule heating effects seen by DE 2, *J. Geophys. Res.*, **93,** 7551-7557.

41. Rich, F J, *& al.* 1987, Using simultaneous particle and field observations on a low altitude satellite to estimate Joule heat energy flow into the high latitude ionosphere, *Ann. Geophys.*, **5,** 527-534.

42. Ahn, B-H, *& al.* 1983, The Joule heat production rate and the particle energy injection rate as a function of geomagnetic indices AE and AL , *J. Geophys. Res.*, **88,** 6275.

43. Knipp, D J, *& al.* 1989, Electrodynamic patterns for September 19, 1984, *J. Geophys. Res.*, **94,** 16913-16923.

44. Siscoe, G L & Huang, T S 1985, Polar cap inflation and deflation , *J. Geophys. Res.*, **90,** 543-547.

45. Moses, J J, *& al.* 1989, Polar cap deflation during a magnetospheric substorm, *J. Geophys. Res.*, **94,** 3785-3789.

46. Hones, E W 1976, The magnetotail: Its generation and dissipation, in *Physics of Solar Planetary Environments,* D.J. Williams, Editor, AGU, Washington, D.C., 558.

47. Hones, E W, *& al.* 1984, Structure of the magnetotail at 220 RE and its response to geomagnetic activity, *Geophys. Res. Lett.*, **11,** 5.

48. Slavin, J A, *& al.* 1985, An ISEE 3 study of average and substorm conditions in the distant magnetotail, *J. Geophys. Res.* , **90,** 10875-10895.

49. Slavin, J A, *& al.* 1986, The interplanetary magnetic field during solar cycle 21: ISEE-3/ICE observations, *Geophys. Res. Lett.* , **13,** 513-516.

50. Slavin, J A, *& al.* 1989, CDAW 8 observations of plasmoid signatures in the geomagnetic tail: An assessment, *J. Geophys. Res.*, **94,** 15153-15175.

51. Baker, D N, *& al.* 1987, Average plasma and magnetic field variations in the distant magnetotail associated with near-Earth substorm effects, *J. Geophys. Res.*, **92,** 71-81.

52. Slavin, J A, *& al.* 1990, IMP-8 observations of traveling compression regions: New evidence for near-Earth plasmoids and neutral lines, *Geophys. Res. Lett.*, **17,** 913-916.

53. Hardy, D A, *& al.* 1979, Occurrence of the lobe plasma at lunar distance, *J. Geophys. Res.*, **84,** 72.

54. Christon, S P, *& al.* 1988, Energy spectra of plasma sheet ions and electrons from ~ 50 eV/e to ~1 MeV during plasma temperature transitions, *J. Geophys. Res.*, **93,** 2562-2572.

55. Baumjohann, W, *& al.* 1988, Average ion moments in the plasma sheet boundary layer, *J. Geophys. Res.*, **93,** 11507-11520.

56. Baumjohann, W, *& al.* 1989, Average plasma properties in the central plasma sheet, *J. Geophys. Res.*, **94,** 6597-6606.

57. Kan J R *& al.* 1988, A thoery of substorms: onset and subsidence:, *J. Geophys. Res.*, **93,** 5624-5640.